

## ANALYSIS OF THE STABILITY VARIATION OF A SLOPE CROSSED BY FOREST FIRE

ROMINA SECCI, SERGIO V. CALCINA, GAETANO RANIERI & GABRIELE URAS

Department of Civil Engineering, University of Cagliari, Environmental Engineering and  
Architecture DICAAR, Cagliari, Italy

### ABSTRACT

This paper deals the study of the stability variation of a hill slope crossed by a forest fire. In order to perform the stability analyses, two geotechnical models were derived by the integration of the results of geotechnical surveys (NSPT measurements and direct shear tests) with electrical resistivity tomographies. Classical approach based on Limit Equilibrium Method is used to determine the safety coefficient. Furthermore, the effects of the forest fire on the slope stability have been discussed modifying the 2D models and introducing an ultra-shallow thin layer with the shear strength parameters determined on burned soil samples, collected after the fire crossing. In particular, this analysis has shown a marked reduction of safety factor at the interface between the burned soil layer and the underlying material for both geotechnical models, considering the infinite slope method with several saturation conditions of the shallow layer.

**KEYWORDS:** Electrical Resistivity Tomography, Fire Effect, Geotechnical Modeling, Slope Stability, Soil Erosion

### INTRODUCTION

The assessment of the slope stability can be treated by a basic approach founded on modeling techniques, considering the physical and mechanical laws of force and moment equilibrium. Several studies have documented the collapse susceptibility of slopes through the integration of the results of geotechnical investigations. However, a preliminary analysis requires specific laboratory test in order to determine the principal parameters of the mechanical soil behaviour, together with a careful analysis of the geomorphologic features of the site [1]. This paper deals the spatial variability analysis of the slope stability through mechanical models, derived from the results of laboratory tests and the interpretation of geophysical surveys.

In a first step, many topographical information are taken from the GIS database, i.e. the digital terrain model for the elevation data are analyzed. After the acquisition of the topographic, geometrical and mechanical information it was possible to apply deterministic models, where the collapse mechanism of the ground is simplified by using the Mohr-Coulomb failure criterion and adopting a rigid perfectly plastic constitutive law. Also this study aims at assessing the effects produced by the passage of wildfires on the susceptibility to instability phenomena. In fact, as is well known, the repeated fire transition predisposes to erosion phenomena [2-4] and consequent desertification [5].

However, the direct effect on the mechanical parameters of soils is not clear. The impact of wildfires on soil erosion is supposed to operate through their effect on soil organic matter and, thus, it depends strongly on fire severity. Soil erosion is then little affected by low-severity wildfires but it markedly increases following high-severity wildfires. All burned top soils becomes from strongly to very strongly water repellent [6]. Furthermore, debris flows are usually associated with shallow landslides and are mainly generated during heavy rains on slopes characterized by low or poor vegetation cover that can induce phenomena of instability on localized zones of the slope [7]. Several works shows that the materials mobilized by shallow landslides are the main source of detrital sediments and they can generate successive debris flows or can induce shallow flows with high-level of solid transport [7-12]. Debris flows increase their run-off rate, by

favoring the erosion phenomena in uppermost areas of hill slopes, on slope affected by previous fire passage [13-18]. The fire-related erosion progressively increases the volume of sediment transported towards down slope. Many studies have been conducted in Spain (Pyrenees area) and showed the correlation between the formation of debris flows and the previous passage of wildfires. In addition, this work will provide the basis for sustainable territorial planning because the movements of slope are natural or man-induced phenomena that generate risks [19-22], and therefore it would be necessary to consider such processes in land planning.

## THE STUDY AREA

The site of investigation is located at western boundary of the rift of Campidano, south-western Sardinia, Italy, to the North-West of the urban area of Villacidro. The geological features are constituted by metamorphic rocks (Hercynian basement) overlying granitoid rocks with a sub-horizontal and weakly wavy contact surface. The main geotechnical units of the Monte Omo slope is the Paleozoic bedrock, which consisting, from North to South, of granitic and metamorphic rocks.

This unit is variously weathered, especially in heavily fractured zones. The medium to coarse-grained granite occupies the lower part of the area, gradually passing to the microgranite at the summit. On top of the granite there are the metamorphic schists [23]. The overlying cover deposits result from the progressive accumulation of material fallen down from the top of the slope.

Their geometrical structure is strongly influenced by the morphological features of the area. The material is granular and incoherent, with heterometric and angular clastic or slightly smoothed skeleton, mainly with sandy matrix or sandy-silty-clay fraction, ranging from loose to moderately dense. In the north-eastern side of the slope there are clastic deposits (Holocene) characterized by heterometric and polygenic elements with a predominance of metamorphic clasts (meta-sandstones, meta-siltstones) and granitic rocks. Fires repeatedly flared up in the area of interest in the last decade (last event in August 2012) progressively reducing vegetation cover, so that shallow erosion developed.

This is detectable in situ and through the analysis of historical orthoimages. The first surveys carried out in 2011 and 2012, in the month of September after the forest fire, put in evidence widespread shallow erosion forms, especially where vegetation had been the eradicated (Figure 1a). The upper top soil layer, 20-50 cm thick, mainly consisted of ash, resulting from vegetation combustion. The last event dating back to August 2012 is classified from high to moderate soil burn severity [24] and has produced extensive damages to the cover vegetation (Figure 1b).

The reduced stabilization effect of the vegetation and subsequent heavy rains have encouraged instability phenomena of shallow layers along the slopes. Figure 2 shows some collapse phenomena in correspondence of several road segments. Before the fire crossing the topsoil was low plastic (with plasticity index ranging from 5 to 10) in both upstream and downstream parts of the slope.

The determination of Atterberg limits performed after the wildfire has shown a lowering of the plasticity index in the samples collected in the upper part of the slope, probably due to the partial combustion of organic matrix present in the soil. Conversely, the same analyses carried out on soil samples taken downstream have not shown this effect. Further tests following the rains indicate a significant reduction of the plasticity index (plasticity index not determinable) also around the lower parts of the slope, highlighting the progressive fine matrix erosion performed by the surface water runoff.



Figure 1: (a) Rut Caused by the Uprooting of Trees after the Fire; (b) Fire of August 2012



Figure 2: Some Images of Collapses and Shallow Slope Instability Phenomena Occurred after the Rains (November 2012)

**METHODS**

Geophysical and geotechnical surveying methods are employed to outline the geological features and mechanical parameters necessary to define the geotechnical models of the site. In particular, the electrical resistivity tomography was used to evaluate shallow layer thickness and define bedrock morphology, and the results of non-standard penetration tests and non-invasive surveys were compared. The soil mechanical parameters were obtained by direct shear laboratory tests performed on several soil samples collected in the study area, as shown in Figure 3.

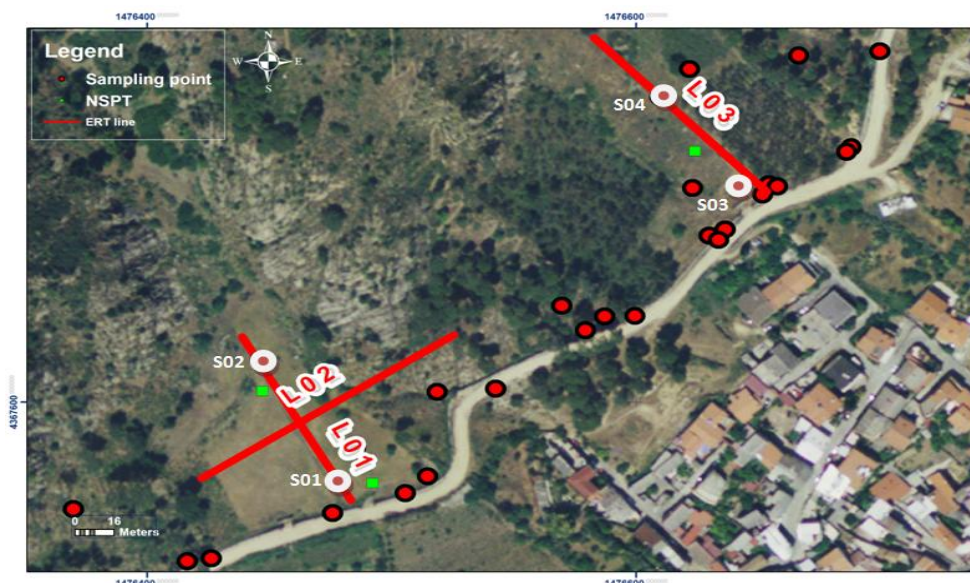


Figure 3: Map of the Study Area with the Locations of the ERT Profiles, the NSPT Measurements and the Soil Sampling Points in Monte Omo Slope

## Geophysical Surveys

Electrical methods are based on electrical resistivity measure of rocks and minerals, which may vary by 20 orders of magnitude [25]. For example, granite rocks are essentially resistive, whereas the resistivity of the shale ranges from 0.5 to 100  $\Omega\text{m}$ . Water saturation increases the conductivity of the geological deposits and can significantly affect its magnitude [26]. Furthermore, different rock types have overlapping resistivity ranges. Subsurface electrical resistivity is measured by placing a quadrupolar device at the free surface. One couple of electrodes sends the current and another couple of electrodes is used for detecting the difference of potential. In recent years, the enhancement of available computer power, together with the development of modern data acquisition tools that enable the multi-electrode management and multi-channel data acquisition (contributing to greatly reduce the acquisition time) and the implementation of numerical inversion procedures [27-29], have encouraged the exploitation of tomographic techniques, permitting to achieve the resistivity sections starting from apparent resistivity pseudo-sections. This result is obtained by an iterative calculus, with progressive minimization of an appropriate object-function. Electrical Resistivity Tomography (ERT) for subsurface imaging employs surface electrode arrays to measure the resistivity distribution in soil and rock. In this study, 2D ERT was applied to investigate the morphology and depth of the bedrock at the interest site.

Thus, this work aims at reconstructing different 2D models, crossing the slope longitudinally and transversely, in order to assess the thickness of the shallow sediments, by associating the different ranges of resistivity to the geological materials in the subsurface. ERT surveys were performed by using the resistivity-meters Syscal-Pro (Iris Instruments) with 10 acquisition channels, with high input impedance (100 M $\Omega$ ), explicitly designed for geophysical applications. Geoelectrical survey was carried out along three straight lines, shown in Figure 1. Each electrical line consists of 48 electrodes, equally spaced and positioned at the distance of 2 m. The acquisition sequences have been optimized to speed up the data acquisition. In order to compare the results obtained with different quadrupole arrays, apparent resistivity measurements were performed along each profile by using both Dipole-Dipole and Wenner-Schlumberger configurations. The data inversion of apparent resistivity was preceded by a series of operations aimed eliminating excessively noisy measurements (such as de-spiking, removal of negative pseudo-resistivity values, etc.), in order to enhance the convergence process and to reduce the difference between the experimental data and the model resistivity values, computed at the end of the  $i^{\text{th}}$  iteration. The 2D electrical data were inverted by using the smoothness-constrained least-squares method [30, 31]. This technique aims at minimizing the square of the changes in the model resistivity values ( $L_2$ -norm optimization method), by producing a model characterized by smooth resistivity variations. The finite-element method was used to solve the forward problem. During the inversion process the node positions were adjusted to take into account the contribution of the topographic irregularities.

The measured data set comprised about 465 values collected from every 2D pseudo section for Wenner-Schlumberger array and 570 values for Dipole-Dipole configuration. Good convergence between the observed data and model resistivity data was obtained after five or six iterations as indicated by the root mean square error misfit values. The resulting 2D resistivity model, relative to L01 line in Figure 4, highlights several important geological features of the subsurface. There is an ultra-shallow layer characterized by resistivity values greater than 2,000  $\Omega\text{m}$  with thickness from 1 to 2 meters, probably consisting of heterometric deposits and erratic blocks. These high resistivity values are probably related to the presence of dry and aerated materials at the ground surface. The second layer shows resistivity values ranging from 200 to 800  $\Omega\text{m}$ , in accordance with the presence of zones characterized by intense alteration of the bedrock or by the shallow debris covers. Major depths are characterized by a more important resistivity gradient, associated with the bedrock transition (with resistivity greater than 2,000  $\Omega\text{m}$ ).

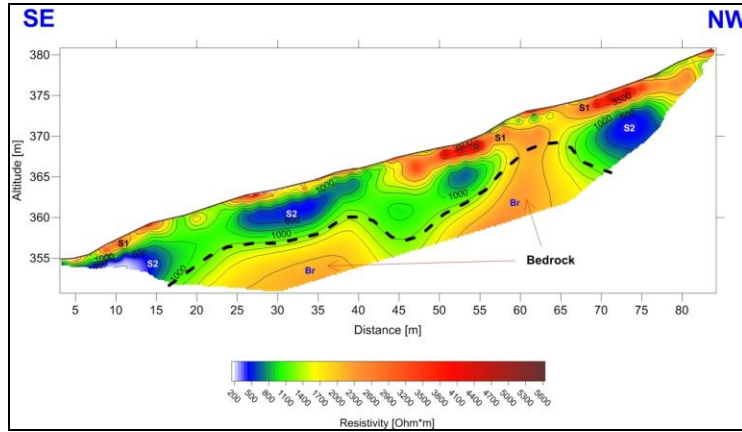


**Figure 4: 2D Electrical Resistivity Tomography with Residual RMS Error of 2.4 % Generated from Extended Survey Line L01 (Wenner-Schlumberger Array)**

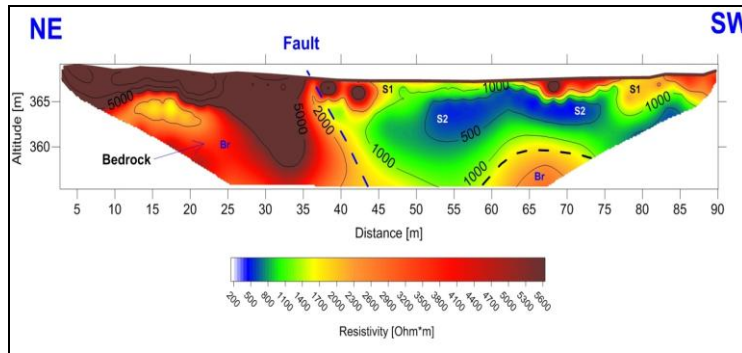


**Figure 5: 2D Electrical Resistivity Model with Residual RMS Error of 3.0 %, Generated from Line L02 (Wenner-Schlumberger Array)**

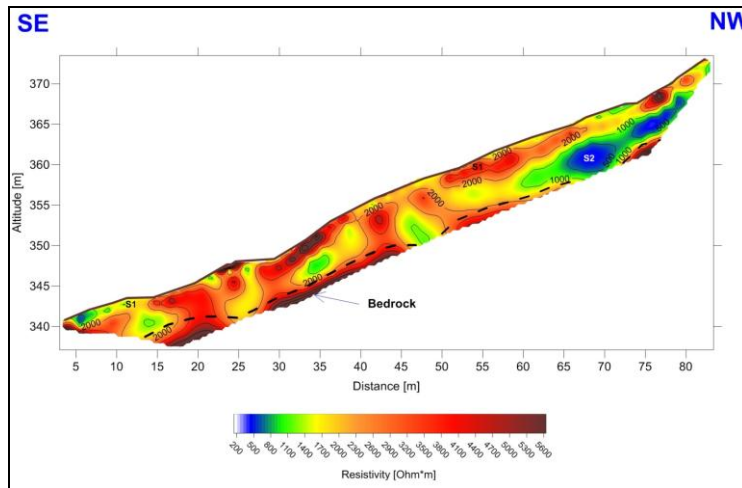


**Figure 6: 2D Electrical Resistivity Model with Residual RMS Error of 5.6 % for the Line L03 (Dipole-Dipole Array)**

The black dashed line plotted in Figure 3 denotes the supposed interface with the intact granitic bedrock. A clear deepening of bedrock can be observed in the central part of the electrical profile. The 2D model along the L02 line, crossing the L01 line at the electrode 24, shows a strong resistivity lateral contrast. In accordance with the surface geological observations this resistivity anomaly is related to the structural features of the granite basement. In particular, the blue dashed line, plotted in Figure 5, is interpreted as a normal fault. Also in this model there is the same uppermost resistive layer correlated with coarse and dry materials with thickness ranging from 0.5 to 2 meters. Whereas the L03 model plotted in Figure 6 shows a more complicated resistivity distribution. In particular, there is the same shallow

high-resistive layer with variable thickness of 2-3 meters but the second layer is more resistive than the previous cases with minimum resistivity values at the higher altitude (around 500  $\Omega\text{m}$ ). At depths between 4 and 8 meters the resistivity values exceed 2,000-3,000  $\Omega\text{m}$ , in agreement with bedrock presence.

### Geotechnical Surveys

In the same slope geotechnical surveys were carried out so as to provide the physical properties (parameters of mechanical behavior) of the soils. In particular, three dynamic non standard penetration tests were performed by using a lightweight penetrometer (with mass of 30 kg and drop height 0.20 m). The soil samples, collected for laboratory testing, were used for grain-size analysis and soil classification. Also, direct shear tests were performed to define the failure parameters (friction angle  $\phi'$  and cohesion  $c'$ ). The attributes of the soil samples are collected and summarized in Table 1. In particular, the samples V01 and V02a were taken at the points S01 and S02 before the fire crossing, at depth about 1.2 and 0.3 m from surface. Conversely the sample V02b was collected near the point S02 in the upper part of the slope affected by the effects of the fire, along the ERT L01. However, along the slope where the ERT L03 was acquired, two samples were collected, the sample V03 before the wildfire and sample V04 after the fire, in the burned area. It is possible to observe that the data relative to soil samples taken after the fire passage show the reduction of the cohesion term with an increase of the friction angle. In other words the materials would assume a prevalent frictional behavior with respect to the previous condition. However, this effect is only confined to a very shallow layer with thickness of about 0.5 meters.

**Table 1: Shear Strength Parameters of the Soil Samples Collected along the Slope of Villacidro, before and after the Fire Crossing**

Soil Sample ID	Friction Angle [ $^{\circ}\text{Sess.}$ ]		Cohesion [kPa]		Unit Weight [ $\text{kN/m}^3$ ]		Depth [m]	Sampling Point ID
	Pre	Post	Pre	Post	Pre	Post		
V01	34.0		16.39		19.02		1.2	S01
V02a	33.6		23.87		18.30		0.3	S02
V02b		36,1		12,06		19.35	0.3	S02
V03	32.0		25.78		18.16		1.0	S03
V04		36.0		11.01		18.00	0.3	S04

## RESULTS

The static analysis of the slope was performed by using the Limit Equilibrium Method of Slices. This approach to the stability assessment was dealt assuming the soil rigid perfectly plastic constitutive law and through the Mohr-Coulomb failure criterion. To determine the circular critical sliding surface (corresponding the minimum safety factor SF), the analysis of stability is performed for several concentric circles with different radius. The minimum value is found plotting each determined safety factor SF in function of the relative radius. This number is the minimum safety coefficient related to the common center of the circles considered. Repeating the same procedure for different center positions a safety factor contour lines map can be drawn. If this surface shows multiple minima means that there are more potential critical failure surfaces.

The inverted electrical tomography together with non standard penetration tests, were able to give us the 2D subsurface models. By associating the shear strength parameters obtained from laboratory testing with their respective materials, the safety factor was determined by considering different sliding surfaces: plane (infinite slope method), circular (Fellenius and Simplified Bishop's methods) and with irregular shape (Simplified Janbu's method). Moreover, without changing the geometric features of the models, the simulations were repeated by inserting the mechanical parameters

obtained for the soil samples taken after the wildfire passage, by introducing in the models an ultra-shallow layer about 0.50 m thick, which simulates the fire effect on the uppermost soil. These methods differ for the several assumptions about the forces acting on the sides of the slices. In particular, the Fellenius or Ordinary method ignores both interslice shear and interslice normal forces and satisfies only the moment equilibrium. This method is conservative because it leads to an underestimation of the safety factor compared to the solutions obtained by other more accurate methods. Other methods are variations and refinements of the Ordinary Method of Slices. The Simplified Bishop Method includes interslice normal forces but ignores interslice shear forces. Also in this case only the moment equilibrium is satisfied. Whereas, the Simplified Janbu Method is similar to the Bishop Method because it includes the interslice normal forces and ignores only the interslice shear forces. The difference between the Bishop and the Janbu Methods is that the second satisfies only the horizontal force equilibrium, as opposed to the moment equilibrium.

These methods were applied in this work to determine the critical safety coefficient with circular arc failure. The minimum safety coefficients are stored in Table 2. However, the obtained results do not show a significant safety coefficient change between the original model and the modified model to take account of the altered material after the fire passage.

**Table 2: Minimum Safety Factor for L01 and L03 Slope Models, before and after the Fire Crossing**

	Ordinary		Bishop		Janbu	
	Pre	Post	Pre	Post	Pre	Post
<b>Model L01</b>	3.083	3.049	3.962	3.906	3.700	3.652
<b>Model L03</b>	2.299	2.291	2.417	2.412	2.261	2.252

The slope extends for a relatively long distance with a consistent subsurface profile so that it may be analyzed as an infinite slope. The failure surface was assumed parallel to the slope surface and the limit equilibrium method could be applied. If a saturated slope is characterized by the seepage parallel to the topographical surface, the same limit equilibrium theory may be applied to determine the safety coefficient. However, in this condition SF depends on the effective normal force and the effective shear strength parameters  $c'$  and  $\phi'$  are used. If the seepage line is assumed to be located at a normalized height  $m$ , above the failure surface, SF is given by the following equation:

$$SF = \frac{c' + [(1 - m)\gamma + m\gamma']h \cos^2(\beta) \tan(\phi')}{[(1 - m)\gamma + m\gamma_{sat}]h \cos(\beta) \sin(\beta)} \quad (1)$$

where  $m = h_w/h$  and  $\gamma' = \gamma - \gamma_w$ ,  $\gamma$  and  $\gamma_{sat}$  are the soil unit weight and the saturated soil unit weight and  $\gamma_w$  is the water unit weight respectively.

This method was applied to estimate the safety coefficient at the interface between the ultra-shallow layer, affected by the fire effects, and the underlying materials. Furthermore, in order to consider the topographic effect, the SF coefficient was determined as slope function. Several saturation conditions of the surface layer were assumed with parallel seepage flow to the sliding flat surface. The results obtained for both L01 and L03 models show high values of safety coefficient, varying from 2.9 to 21.8 for profile L01 and from 2.4 to 14.5 for profile L03.

However, the comparison between the SF values, derived before and after the wildfire, shows a significant reduction between the two different conditions. An example of safety factor calculated with the above equation is shown in Figure 7, where it is possible to observe the difference between the solid function, which denotes the SF before the wildfire for several  $m$  values and the dashed function, which indicates the SF computed by using the shear strength parameters of the burned soil.

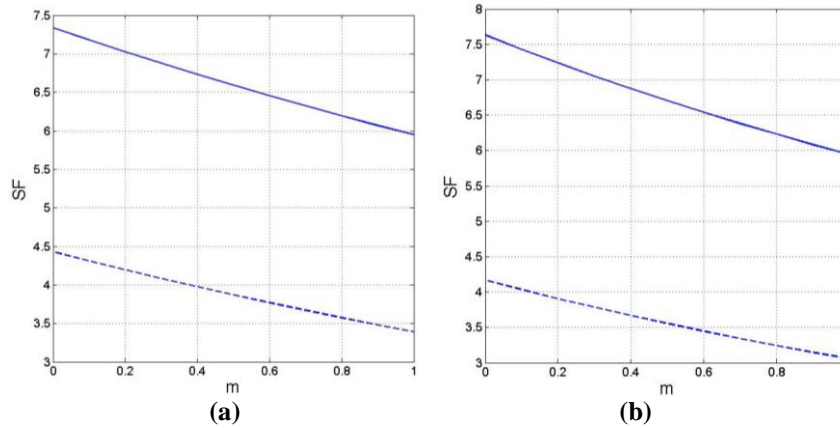


**Figure 7: Examples of the Safety Factor for the Same Slope Gradient as Function of m Parameter before (Solid Line) and after (Dashed Line) the Fire Passage for L01 Profile (a) and for L03 Profile (b)**

Figure 8 shows the trend of the percentage relative variation of the stability factor in relationship to the slope inclination. The variation percentage, calculated according to the following expression:

$$\Delta SF[\%] = \frac{SF_{Pre} - SF_{Post}}{SF_{Pre}} \cdot 100 \quad (2)$$

highlights that the reduction of the stability coefficient ranges between 37.5 and 44 % for the profile L01 and from 42.5 to 51.5 % for the profile L03. Furthermore, this trend increases with the gradient of slope.

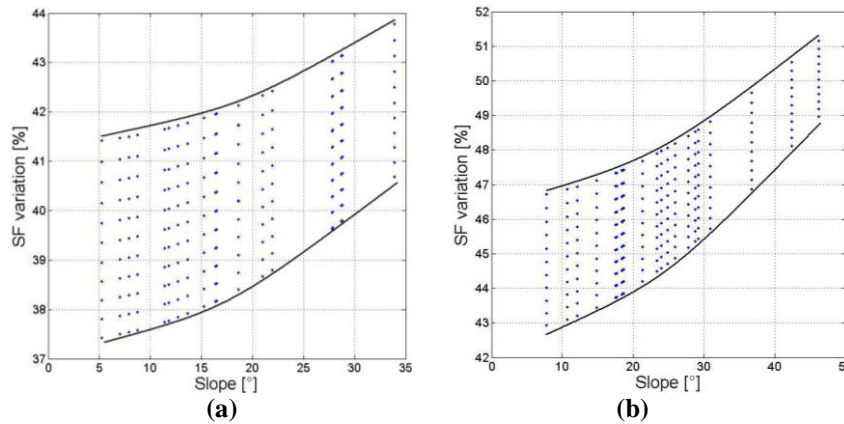


**Figure 8: Percentage Reduction of the Safety Factor SF for Different Slope Angles between m=0 (Dry Soil) and m=1 (Saturated Soil) Considering a Parallel Seepage to the Sliding Surface, Respectively for L01 Profile (a) and for L03 Profile (b)**

## CONCLUSIONS

The results of the geophysical survey indicate that the topsoil is within a depth range up to 2 m and it is characterized by high-resistivity values which indicate dry and detritic materials. The second layer is within the depth range between 2 and 8 m with resistivity varying from 200 to 800  $\Omega\text{m}$ . The third geoelectric layer is the bedrock having resistivity values higher than 2,000  $\Omega\text{m}$ . The results of the electrical resistivity tomographies are well correlated with the dynamic penetration tests. Furthermore, the 2D resistivity surveys have provided valuable information on the lateral and vertical variation of the bedrock basement. The features of the slope have been analysed with geotechnical tests before and after the fire passage. The results of direct shear tests performed on burned soil samples show a partial reduction of the cohesion, with respect to the original material, together with a weak increase of the friction angle. In particular, the infinite slope method proved effective in highlighting the reduction of safety factor at the interface between the surface soil,

affected by the effects of the combustion, and the base material. Further information can be achieved by enhancing the study with additional geotechnical and geophysical analysis and by verifying quantitatively the increase of the erosion degree in this area and in other zones affected by the same phenomena.

## ACKNOWLEDGEMENTS

Authors would like to thank L. Noli and M. Sitzia for their contribution to the field work.

Sergio Calcina gratefully acknowledges Sardinia Regional Government for the financial support of her PhD scholarship (P.O.R. Sardegna F.S.E. Operational Programme of the Autonomous Region of Sardinia, European Social Fund 2007-2013 - Axis IV Human Resources, Objective 1.3, Line of Activity 1.3.1.)”.

## REFERENCES

1. Duncan, J.M., 1996. State of art: limit equilibrium and finite-elements analysis of slopes. *J. of Geotechnical Engineering, ASCEE*, 122, 7, 557-596.
2. González-Pelayo, O., Andreu, V., Campo, J., Gimeno-García, E., Rubio, J.L., 2006. Hydrological properties of a Mediterranean soil burned with different fire intensities. *Catena*, 68, 186 – 193.
3. González-Pelayo, O., Andreu, V., Gimeno-García, E., Campo, J., Rubio, J.R., 2010. Effects of fire and vegetation cover on hydrological characteristics of a Mediterranean shrubland soil. *Hydrological Processes*, 24, 1504–1513.
4. Shakesby, R.A., 2011. Post-wildfire soil erosion in the Mediterranean: Review and future research directions. *Earth-Science Reviews*, 105, 71–100.
5. Fernández, C., Vega, J.A., Vieira, D.C.S., 2010. Assessing soil erosion after fire and rehabilitation treatments in NW Spain: performance of rusle and revised morgan–morgan–finney models. *Land Degrad. Develop.*, 21, 58–67.
6. Varela, M. E., Benito, E., Keizer, J.J., 2010. Wildfire effects on soil erodibility of woodlands in NW Spain. *Land Degrad. Develop.*, 21, 75–82.
7. Blijenberg, H., 1998. Rolling stones. Triggering and frequency of hillslope debris flows in the Bachelard Valley, Southern French Alps. Utrecht University, Utrecht.
8. Johnson, A.M., Rodine, J.R., 1984. Debris flow, Slope instability, Wiley, Chichester.
9. Lorente, A., García-Ruiz, J.M., Beguería, S., Arnáez, J., 2002. Factors explaining the spatial distribution of hillslope debris flows. A case study in the Flysch Sector of the Central Spanish Pyrenees. *Mountain Research and Development* 22, 32–39.
10. Lorente, A., Beguería, S., Bathurst, J.C., García-Ruiz, J.M., 2003. Debris flow characteristics and relationships in the Central Spanish Pyrenees. *Natural Hazards and Earth System Sciences*, 3, 683–692.
11. Beguería, S., 2006. Changes in land cover and shallow landslide activity: a case study in the Spanish Pyrenees. *Geomorphology*, 74, 196–206.
12. Bathurst, J.C., Moretti, G., El-Hames, A., Beguería, S., García-Ruiz, J.M., 2007. Modelling the impact of forest loss on shallow landslide sediment yield, Ijuez catchment, Spanish Pyrenees. *Hydrology and Earth System Sciences*, 11, 569–583.

13. Cannon, S.H., Kirkham, R.M., Parise, M., 2001a. Fire-related debris flow initiation processes, Storm King Mountain, Colorado. *Geomorphology*, 39, 171–188.
14. Cannon, S.H., Bigio, E.R., Mine, E., 2001b. A process for fire-related debris flow initiation, Cerro Grande fire, New Mexico. *Hydrological Processes* 15, 3011–3023.
15. Cannon, S.H., Gartner, J.E., Rupert, M.G., Michael, J.A., Rea, A.H., Parrett, C., 2010. Predicting the probability and volume of post wildfire debris flows in the intermountain western United States. *Geological Society of America Bulletin*, 122, 127–144.
16. Gabet, E.J., 2003. Post-fire thin debris flows: sediment transport and numerical modeling. *Earth Surface Processes and Landforms*, 28, 1341–1348.
17. Parise, M., Cannon, S.H., 2011. Wildfire impacts on the processes that generate debris flows in burned watersheds. *Natural Hazards*. doi:10.1007/s11069-011-9769-9.
18. García-Ruiz, J.M., Arnáez, J., Gómez-Villar, A., Ortigosa, L., Lana-Renault, N., 2012. Fire-related debris flows in the Iberian Range, Spain. *Geomorphology*, accepted 27 March 2012.
19. Varnes, D.J., 1984. Landslides hazard zonation: a review of principles and practice. UNESCO, Paris, 63.
20. Fell, R., 1994. Landslide risk assessment and acceptable risk. *Canadian Geotechnical Journal*, 31, 261-272.
21. Glade, T., 2005. Linking debris-flow hazard assessments with geomorphology. *Geomorphology*, 66 (1), 189-213.
22. Chacon, J., Irigaray, C., Fernandez, T., El Hamdouni, R., 2006. Engineering geology maps: landslides and geographical information systems. *Bulletin of Engineering Geology of the Environment*, 65, 341-411.
23. Barrocu, G., Houtkamp, H., Jacks, L., Larsson, I., 1974. Geohydrological investigations of ground water in granite rocks of Sardinia."Rep. Inst. för Kulturteknik", 1-74, Stockholm.
24. Parsons, A., Robichaud, P. R., Lewis, S. A., Napper, C., Clark J. T., 2010. Field guide for mapping post-fire soil burn severity. General Technical Report RMRS-GTR-243, USDA, 49 pp.
25. Grant, F.S., West, G.F., 1965. Interpretation theory in applied geophysics, McGraw-Hill, New York.
26. Telford, W.M., Geldart, L.P., Sheriff, R.E., 1990. Applied Geophysics, Cambridge University Press, Cambridge.
27. Loke, M.H., Barker, R.D., 1996a. Practical techniques for 3D resistivity surveys and data inversion. *Geophys. Prospec.*, 44, 499-523.
28. Loke, M.H., Barker, R.D., 1996b. Rapid least-squares inversion of apparent resistivity pseudosections by a quasi-Newton method. *Geophys. Prospec.*, 44, 131-152.
29. Dahlin, T., 2001. The development of DC resistivity imaging techniques. *Computers & Geosciences*, 27, 1019-1029.
30. DeGroot-Hedlin, C., Constable, C., 1990. Occam's inversion to generate smooth two-dimensional models from magnetotelluric data. *Geophysic*, 55, 1613-1624.
31. Sasaki, Y., 1992. Resolution of resistivity tomography inferred from numerical simulation. *Geophysical Prospecting*, 40, 453-464.